

Omega meson electroproduction analysis

D A Unwuchola¹, S H Connell¹, P E Bosted² and JLab Hall C²

¹ University of Johannesburg, Johannesburg, South Africa

² Thomas Jefferson National Accelerator Facility, Newport News, VA 23606, USA

E-mail: doomnull@gmail.com

Abstract. The electroproduction process $p(e, e'\omega)p$ has been measured at $Q^2 \sim 5.5$ (GeV/c)² in Jefferson Lab's Hall C. Considering the process, $\gamma^*p \rightarrow p'\omega$, the unpolarised differential cross sections are reported. Discussions are made on various details relating to the background subtractions, radiative corrections and systematic errors. The ω extracted cross section seems stronger when compared with an extrapolated input cross model using the dipole form factor $G = (1 + \frac{Q^2}{0.71})^{-2}$. There are significant evidence of resonance formation in this reaction channel.

1. Introduction

With only few measurements of the cross section of ω mesons electroproduction in the near threshold regime, the high intensity of the CEBAF beam combined with the large acceptance of CLAS allows us to perform measurement with an unprecedented accuracy in JLab [1][2]. In the work presented here, our main goal is to measure the exclusive ω differential cross section in the highest achievable Q^2 values in the valence quark region. Through this we can get information about the relative strength of the multiple and overlapping high resonance for the process $p(e, e'\omega)p$ at the average Q^2 of 5.5 GeV². This in turn could be use in the extraction of information to better understanding of the structure of the isospin 1/2 resonances for the $p\omega$ channel preferred to other channels. The detailed analysis can be found in Ref. [3].

2. Experiment

For the present analysis, the data were acquired in Hall C at the Thomas Jefferson National Accelerator Facility (JLab) during an experiment also design to study electroproduction of η and π^0 in the reactions $p(e, e'p)\eta$ and $p(e, e'p)\pi^0$ respectively [4][5]. The instrumentation layout of the experiment can be found also in Refs. [3]. The E01-002 experiment basically consists of an electron beam energy of 5.5GeV incident on a cryogenic target, two spectrometers for detecting negative and positive particles, and electronics with softwares for reconstruction of events.

The scattered electrons were detected using the Short Orbit Spectrometer (SOS)[6][7], a resistive $QD\bar{D}$ (quadrupole, dispersive dipole, anti-dispersive dipole) spectrometer while the High Momentum Spectrometer (HMS), $QQQD$ spectrometer, was used in detecting the recoil protons. The ω particles were identified using the missing mass method.

At each of the Q^2 points, the electron spectrometer was fixed in both angle and momentum, and so defining a central three-momentum transfer \mathbf{q} . The direction of a boosted decay cone of protons is determined in turn by the vector \mathbf{q} . In other to capture as much of this decay cone possible, the proton spectrometer was stepped in angle and momentum, with kinematics

chosen such that adjacent settings overlapped in the mentioned two variables [8]. With such approach, there is reduction in systematic uncertainties associated with imperfect knowledge of the spectrometer acceptance. The Kinematic settings of the data is shown in table 1

Table 1. Spectrometer settings for the $Q^2 \approx 5.36 \text{GeV}^2/c^2$, ($E = 5.5 \text{GeV}$) data.

Electron Arm $P_{SOS}[\text{GeV}/c]$	Electron Arm $\theta_{SOS}[\text{degrees}]$	Proton Arm $P_{HMS}[\text{GeV}/c]$	Proton Arm $\theta_{HMS}[\text{degrees}]$
1.74	47.5	2.13	13.5, 16.5, 19.5, 22.5
1.74	47.5	2.23	18.0, 12.0, 15.0, 21.0
1.74	47.5	2.57	11.2, 13.5, 16.5, 19.5, 22.5
1.74	47.5	2.69	12.0, 15.0, 18.0, 21.0, 24.0
1.74	47.5	3.10	11.2, 13.5, 16.5, 19.5, 22.5
1.74	47.5	3.24	12.0, 15.0, 18.0, 21.0, 24.0
1.74	47.5	3.73	11.2, 13.5, 16.5, 19.5, 22.5
1.74	47.5	3.90	12.0, 15.0, 18.0, 21.0
1.74	47.5	4.50	11.2, 13.5, 16.5, 19.5
1.74	47.5	4.70	15.0, 18.0

The electron spectrometer (SOS) was used to separate the electrons from the negatively charged pions. This was done by using a threshold gas Čerenkov detector and a lead-glass calorimeter. In the High Momentum Spectrometer (HMS), protons were separated from positively charged pions using a combination of coincidence time (the difference between the trigger times of two the spectrometers) and particle velocity, or the time of flight β_{tof} .

3. Data Analysis

The Hall C analysis code called ENGINE was used for the offline data analysis of the collected raw signals. This analysis code, written in Fortran computer language, reads each of the events, determines which detectors were fired, reconstructs trajectories, and also generates particle identification information for each event. In essence, the replay ENGINE converts raw data into calibrated physical quantities on an event by event basis. These physical quantities may include combinations of raw data quantities. Also developed were other analysis codes making use of Perl and C++ in the Root Data Analysis framework.

For reliable results from our data, corrections were done on a run-by-run basis. These corrections were done on the track reconstruction inefficiencies, dead times and also on offsets. All the corrections applied to the data are shown in table 2. The experimental offsets are as a result of lack of consideration of the uncertainties in the fittings of the reconstruction matrix elements for the spectrometers. The calculation of the experimental cross sections is dependent on physics quantities (e.g Q^2 and W) obtained from the reconstructed spectrometer quantities (central angles and momenta) and the beam energy. This resulted to it being directly sensitive to the uncertainties in the spectrometer quantities. Enlisted in table 3 are the entire set of kinematic offsets that were used during the replay of our present data.

Proton absorption is one of the main contributors on the trigger efficiency. The condition for a proton to cause a trigger in the HMS is that it had to deposit enough energy to create above-threshold signals in at least three out four scintillator planes in the detector stack. A trigger inefficiency for proton detection in the HMS is produced by protons which are not detected in their interaction with the scintillator and by protons that do not make through all

Effects	Correction in %
Proton absorption	$+4 \pm 1$
[†] Computer dead time	$+(1.0 - 19.1)$
[†] HMS tracking	$+(2.3 - 14.3)$
[†] SOS tracking	$+(0.3 - 0.9)$
[†] Electronics dead time	$+(0.0 - 2.4)$
[‡] Random coincidence	$-(0.0 - 7.6)$

Table 2. Corrections applied to the data. Indicated by the parentheses are the range of correction sizes applied on a [†]run-by-run or a [‡]bin-by-bin basis.

Quantity	HMS	SOS
θ	0.0 ± 0.5 mrad	0.0 ± 0.5 mrad
ϕ	$+1.1 \pm 0.5$ mrad	$+3.2 \pm 0.5$ mrad
p	-0.13 ± 0.05 %	-1.36 ± 0.05 %
E_e	0.00 ± 0.05 %	0.00 ± 0.05 %

Table 3. Kinematic offsets applied to the data during the replay phase.

the scintillators due to absorption. A correction of 4 % was applied to the data due to proton absorption. A further description on the trigger efficiency is found in Ref. [4].

The radiative corrections for our experiment were done within SIMC using the formalism of Ent, which is a general framework for applying radiative corrections in $(e, e'p)$ coincidence reactions at GeV energies [4]. The size of the radiative corrections implemented by SIMC is done by running the full simulation with and without including radiative effects as shown in Figure 1. The uncertainty in the radiative corrections was estimated to be 2%.

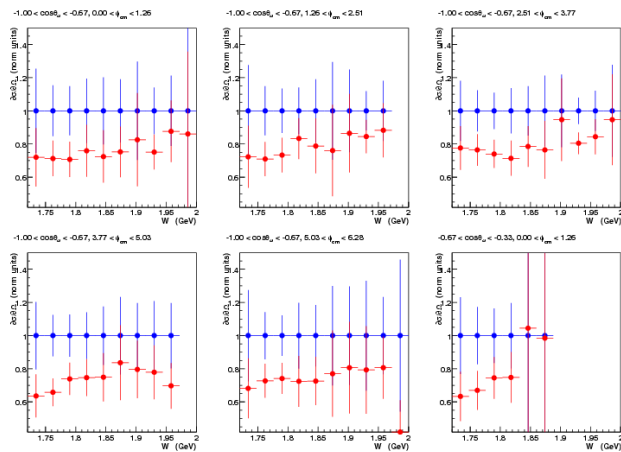


Figure 1. (Colour online) Plots running SIMC with (blue) and without (red) radiative effects for selected $\cos\theta_\omega$ and ϕ_{cm} . Both Plots were normalised to the plots on running with SIMC (blue).

In inelastic scattering, the detection of scattered electron and recoil protons is not an exclusive measurement. That is, there would be at least one other emitted particle. With only one undetected particle, we reconstructed the kinematics of that particle in which in our case was through the channel, $p(e, e'p)\omega$. This was done by constructing the square of the missing mass m_x^2 which involved the use of energy and the four-momentum conservation. The extraction of ω resulted in applying a cut on m_x^2 around the omega peak and subtracting the background.

The background is due to event with more than one undetected particle. What we observed in this case is that the missing mass did not correspond to any physical mass. This was because the mass of the missing momentum was smaller than the sum of the magnitudes of the individual momenta of the undetected particles. Predominantly this production were multiple pions which were the principle background in this experiment. The treatment of the background was done by simulating the m_x^2 spectra of the background using SIMC with a model of the largest contributing reactions, which basically involved pions, from the data. With this output of the simulation being a large set of multipion events that were accepted in our detectors, these events were then filled of the same structure as those of the data. Consequently, these yielded our approximation to the shape of the multipion background without an absolute normalisation. As an absolute multipion cross section was not being extracted, the shape was sufficient to subtract it from the data. Indicated in Figure 2 was Monte Carlo simulation with multipion background also simulated.

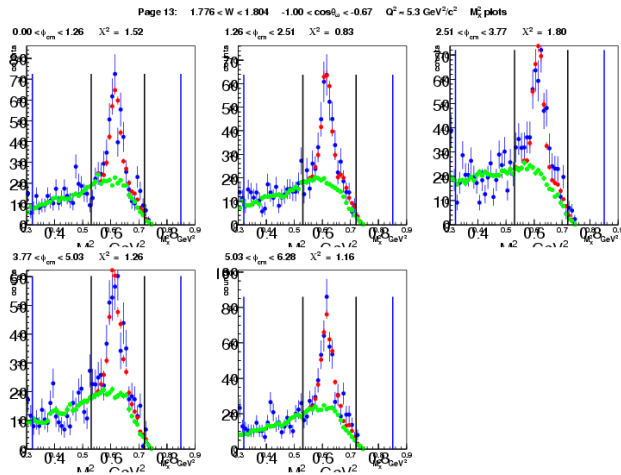


Figure 2. (Colour online) A Selected missing mass squared plots indicating both Monte Carlo simulation (red) and data (blue) and two cuts to select the ω peak. Simulation of multipion background (green) was now included in these selected plots. The dark line indicated the region within which the ω cross-section was extracted and the blue line indicated the indicated the region within which the background fit was done.

With the method of a two-parameter fit in each $(W, \cos\theta_\omega, \phi_\omega)$ bin, the background to data was normalised in the simplest way. The consequence of this is that the m_x^2 spectra of the multipion background simulation and the ω simulation production would had been normalised in order to minimise the χ^2 difference between their sum and data m_x^2 spectrum. However, what was observed, due to diminishing acceptance, was that the out-of-plane ϕ bins demonstrated a phenomenon where the multipion background simulation and the ω production simulation could have m_x^2 spectra similar enough to make a two-parameter fit unreliable. Typically, this was observed in $\cos\theta_\omega$ outside -1.00 and -0.67, and worsened as W increased.

As a result of this, the fit was constrained to have the multipion normalisation parameter constant over ϕ_ω , as expected physically. The effect of other particles which produced radiation tail, in principle, under the ω peak was neglected as the size of this effect was so small when compared to the uncertainty in the multipion background. This approach gave an acceptable outcome in the reproduction of the shape of the measured m_x^2 spectra. As could be seen, the sum of the normalised simulation seemed to match the data well. Shown in Figure 2 are a few representative spectra showing the W and $\cos\theta_\omega$ dependence of the missing of the m_x^2 distributions. The uncertainty in the normalised background simulation was determined by adding small Monte Carlo statistical uncertainty to the Minuit [9] fit uncertainty on the normalisation parameter in the quadrature.

Shown in table 4 are the set of 'standard' cuts applied to the data. Cuts such as the particle momentum deviation at both the SOS and HMS (δ_h and δ_s) were applied to ensure that only particles within the understood region of the spectrometer momentum acceptance were

used. Also used, but not listed in table 4, were cuts on the collimators at both spectrometers [5]. These were to ensure that the path of the reconstructed track of a detected particle traced back through acceptable regions of the collimator slits.

Table 4. Set of 'standard' cuts applied to the data and to the simulation where applicable. [†] The particle Identification cuts were not applied to the simulation.

Quantity	Cut	Purpose
[†] Coincidence time	$ t_{coin} - t_{cent} \leq 1.5$	Selecting proton
HMS particle momentum deviation, $\delta_h = \frac{P - P_{HMS}}{P_{HMS}}$	$ \delta_h \leq 9\%$	HMS acceptance
SOS particle momentum deviation, $\delta_s = \frac{P - P_{SOS}}{P_{SOS}}$	$-15\% \leq \delta_s \leq +20\%$	SOS acceptance
SOS x position focal plane, $X_{SOS,f,p}$	$-20cm \leq X_{SOS,f,p} \leq +22cm$	SOS acceptance
[†] SOS shower counter sum, E_{norm}	$E_{norm} \geq 0.7$	selecting electron
[†] SOS Čerenkov number of photons, $N_{p.e.}$	$N_{p.e.} \geq 0.5$	selecting electron
Missing mass squared m_x^2	$0.56 \text{ GeV}^2 \leq m_x^2 \leq 0.66 \text{ GeV}^2$	selecting ω particle

The data were binned in $\{W, \cos\theta_\omega, \phi_{cm}\}$ for the purpose of extraction of the cross section as in indicated in table 5. The Monte Carlo method was used to extract the cross section from

Table 5. The ω analysis binning for Experiment E01-002.

Variable	Range	Bins
W (GeV)	$1.72 \leq W \leq 2.0$	10
$\cos\theta_\omega$	$-1.0 \leq \cos\theta_\omega \leq 1.0$	6
ϕ_ω (rad)	$0 \leq \phi_\omega \leq 2\pi$	5

the data which comes out, in practice, with distortions from systematic and random effects that could not be reliably deconvoluted from the data. Instead, a model of the theory was subjected to Monte Carlo procedure which simulated the data in a direction that the model would have led to if it went through the same systematic and random effects as provided by a realistic simulation of the actual experiment (spectrometers, target, beam). In essence, the data yield was obtained, then acquired was the Monte Carlo yield which was followed with obtaining these yields ratio and finally scaling the measured experimental cross-section from the obtained ratio.

Our measurement for the reaction $p(e, e'p)\omega$ was also modelled using the MAID 2003 model for electroproduction. This model of lower Q^2 was weighted by the dipole form factor, $G = (1 + \frac{Q^2}{0.71})^{-2}$, and used to extrapolate the ω electroproduction cross-section at high Q^2 . It should be made known that It was the square of this dipole form factor that contributed to the cross-section.

4. Results and Conclusion

Figure 3 displays a set of the computed centre-of-mass differential cross sections for the process $p(e, e'\omega)p$ process on an average Q^2 of 5.5 GeV^2 at the invariant mass range $1.72 \leq W \leq 2.0 \text{ GeV}$ with full coverage of $\cos\theta_{cm}$ and ϕ_{cm} . The cross section was computed in six $\cos\theta_{cm}$ and five ϕ_{cm} bins. This data set is from an extended kinematic region in Q^2 to studies from CLAS [10][2]. For this work done at $W \leq 2.0 \text{ GeV}$, we neglected the ρ meson interference which could produce an asymmetry in the peak, sharper at lower missing mass, and broader at higher missing mass. The ρ interference effect would come into play for works above 2.0 GeV in invariant mass. Our

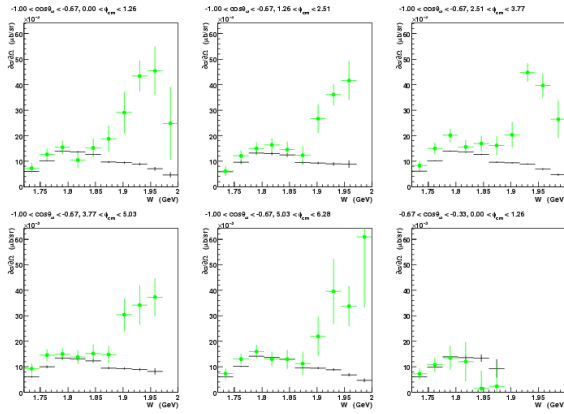


Figure 3. A set of differential cross section with black line indicating the MAID 2003 model input cross section.

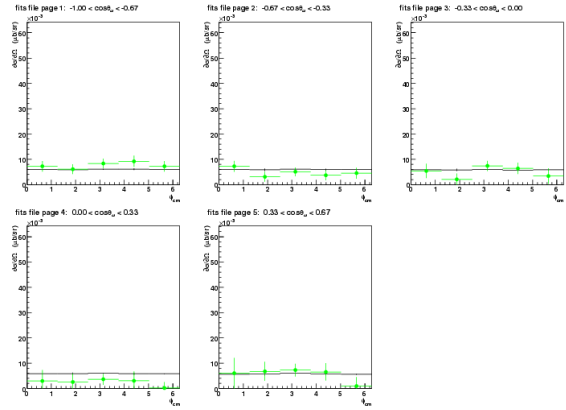


Figure 4. A set of cross section flat in ϕ_{cm} .

extracted cross section seem stronger than the MAID 2003 model cross section extrapolated to 5.5 GeV^2 using the dipole form factor, $G = (1 + \frac{Q^2}{0.71})^{-2}$. Both our cross section and the model peak are more or less the same for $W \leq 1.86 \text{ GeV}$. However, at higher W and more backward angle ($-1.0 \leq \cos\theta_{cm} \leq -0.6$), our data grows stronger, Figure 3. The bumps as can be seen corresponds to regions of resonances. As shown in Figure 4, the cross section seems not to have a significant ϕ_{cm} dependence in the ϕ_{cm} plots for some W bins. The results of the presented measurement of the ω differential cross section are sensitive to high-mass baryon resonances and diverge significantly from the MAID 2003 extrapolation (using the square of the dipole form factor $G^2 = (1 + \frac{Q^2}{0.71})^{-4}$) of the lower Q^2 data. The use of our ω data which is characterized by it backward angular coverage, together with existing data, could enable the Q^2 of the transition form factors into higher mass resonances to be measured. With such measurement, there are rooms for improvement to the understanding of the QCD structure of these resonance regions. Detailed description of the results of the extraction process and the tabulations of the extracted differential cross section with the global systematic error analysis is found in Ref. [3].

I would like to acknowledge the support of the staff and management at Jefferson Lab, and the staff of physics department in the University of Johannesburg.

References

- [1] Ambrozewicz P *et al* 2004 *Phys. Rev. C* **70** 035203
- [2] Laget J M 2004 *Phys. Rev. D* **70** 054023
- [3] Unwuchola D A 2011 *MSc thesis* (University of Johannesburg)
- [4] Dalton M M *et al* 2009 *Phys. Rev. C* **80** 015205
- [5] Villano A N *et al* 2009 *Phys. Rev. C* **80** 035203
- [6] Mohring R M 1999 Ph.D. thesis University of Maryland
- [7] Arrington J R 1998 Ph.D. thesis California Institute of Technology
- [8] Bosted P 2003 Kinematic settings and singles rates for E01-002 Hall C JLab
- [9] James F and Roos M 1975 *Minuit: A system for function minimization and analysis of the parameter errors and correlations.* (Comput. Phys. Commun.) p 343
- [10] Morand L 2005 *European Physical Journal A* **24** 445